*Optica Applicata, Vol. XXIX, No. 1–2, 1999*

# Beam propagation method for analysis of multimode interference structures made by $K^+$-$Na^+$ ion exchange in glass

MAREK BŁAHUT

Institute of Physics, Silesian Technical University, ul. Bolesława Krzywoustego 2, 44–100 Gliwice, Poland.

In the paper, a beam propagation method for analysis of the gradient multimode interference structure made by $K^+$-$Na^+$ ion exchange in glass is presented. Self-imaging phenomena appearing during general and restricted interference are considered as well as a possibility of using ion-exchanged multimode interference structure as 3 dB couplers and $1 \times N$ power splitters is examined.

## 1. Introduction

In recent years there has been observed a growing interest in the application of multimode interference (MMI) structures in basic integrated optic devices: 3 dB couplers and power splitters. Their unique properties such as insensitivity to wavelength and polarization, low loss, small size, and ease of fabrication make MMI structures attractive for advanced applications in Mach–Zehnder switches and modulators, ring lasers, and multiplexers [1]. Designing of such structures for the expected working characteristics can be realized by mathematical modelling. Various approaches using ray optics [2], finite element methods [3], and full modal propagation methods for two and three dimensional case [1], [4] have been discussed for the analysis of MMI step index structures.

In this paper, the finite difference beam propagation method (FDBPM) for the characterization of gradient index MMI structures is presented. Gradient index MMI sections examined are the ion-exchange waveguides made by $K^+$-$Na^+$ ion exchange in glass. The $K^+$-$Na^+$ ion exchange is a popular method of obtaining passive integrated optical elements [5]. A possibility of the application of ion-exchanged MMI structures in the technology of such passive optical elements has not been examined yet. The evolution of the wave fields is considered for the different propagation conditions related to the general and restricted interference. Self-imaging effects and the input field reconstruction in single, mirrored and multiple images are examined. Based on the above, a possibility of using ion-exchanged MMI structures as 3 dB couplers and $1 \times N$ way power splitters is shown.

## 2. Basic concept

A scheme of MMI structure is shown in Figure 1. It consists of a group of monomode waveguides which define the input field and belong to a wide multimode section where the interference effects of modal fields are observed, and the output monomode waveguides.

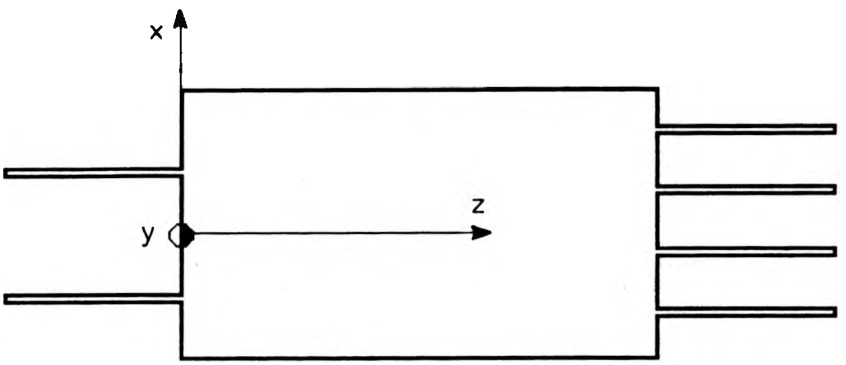


Fig. 1. Schematic diagram of a multimode interference structure.

The monomode waveguides give the stable distribution of the input field $E(x, y, 0)$. This field introduced to the interference section is decomposed into the modal fields $\varphi_{nm}(x, y)$ of all the modes of the multimode waveguide

$$E(x, y, 0) = \sum_{n,m} c_{nm} \varphi_{nm}(x, y) \tag{1}$$

where $\varphi_{nm}$ is the orthogonal wave function of the $(n,m)$ mode with the propagation constant $\beta_{mn}$ and coefficients $c_{nm}$ are defined by the equation

$$c_{nm} = \frac{\int E(x, y, 0) \varphi_{nm}(x, y) \, dx dy}{\sqrt{\int \varphi_{nm}^2(x, y) dx dy}}. \tag{2}$$

The field at the distance $z$ is a superposition of all the modal fields with the different phase shifts

$$E(x, y, z) = \sum_{n,m} c_{nm} \varphi_{nm}(x, y) \exp(-j \beta_{nm} z). \tag{3}$$

Each mode of MMI section propagates with a different phase velocity and hence an interference pattern is produced along the waveguide section. In the case of the quadratic dependence of propagation constants on the mode number so-called self-imaging effects are observed.

The guided-mode propagation analysis requires a detailed calculation of all the model fields and propagation constants. They can be easily determined only for two-dimensional multimode structures. Problems can also appear in the characteri-

zation of MMI structures with a very wide interference section and a big number of modal fields.

A more efficient way of describing the MMI structure, particulary in a three-dimensional case, is the FDBPM technique.

## 3. Finite difference beam propagation method

The beam propagation method is very powerful in simulating the propagation of light in structures which cannot be treated analytically. Assuming TE polarization and a time dependence $\exp(-j\omega t)$, we have in a three-dimensional case

$$\partial^2 E/\partial x^2 + \partial^2 E/\partial y^2 + \partial^2 E/\partial z^2 + n^2(x, y, z)k^2 E(x, y, z) = 0 \tag{4}$$

where $n(x, y, z)$ is the refractive index and $k = \omega/c$. A scalar field distribution $E(x, y, z)$ can be written according to the slowly varying envelope approximation as

$$E(x, y, z) = u(x, y, z)\exp(jkn_0) \tag{5}$$

where $n_0$ is a real reference constant. Substituting it into (4) yields

$$\partial^2 u/\partial z^2 + 2jkn_0 \partial u/\partial z + (\partial^2 u/\partial x^2 + \partial^2 u/\partial y^2 + k^2(n^2 - n_0^2)u = 0. \tag{6}$$

A paraxial or Fresnel equation is obtained from (6) by removing the second order $z$-derivative term

$$-2jkn_0 \partial u/\partial z = (\partial^2 u/\partial x^2 + \partial^2 u/\partial y^2 + k^2(n^2 - n_0^2)u. \tag{7}$$

Equation (7) is solved numerically using the alternating direction implicit method [6] and the Cranck–Nicholson finite difference scheme with transparent boundary conditions [7] at the edge of the computational window. The computational window dimensions are given by $I_x \times I_y = 60\ \mu m \times 15\ \mu m$, the number of transverse grid points is $200 \times 50$ and the step of propagation $\Delta z = 0.5\ \mu m$. In each step of calculations, beginning with the initial field distribution at $z = 0\ \mu m$, the field distribution at propagation step $z + \Delta z$ is expressed in terms of the field at propagation step $z$.

## 4. Gradient-index MMI structure made by $K^+$-$Na^+$ ion exchange

The basic element of the examined MMI gradient index structure is the multimode waveguide made by $K^+$-$Na^+$ ion exchange in glass [8]. In the computational window of Fig. 2, there is presented the distribution profile of the refractive index $\Delta n(x, y)$ in the MMI section. This was obtained in the diffusion process through the opening of the width 36 μm at a time 1 h and calculated numerically from the nonlinear diffusion equation [8]. The substrate is borosilicate glass of the refractive index 1.51 situated at $y = 3\ \mu m$ and surrounded by air. Material parameters of the ion-exchange used in our calculation are: the self-diffusion coefficient of $K^+$ ions $D = 1.64\ \mu m^2/h$, the mobility ratio $r = 0.9$, and the maximum of the refractive index change $\Delta n = 0.0084$. The waveguide is single-mode in the transverse direction $y$ and

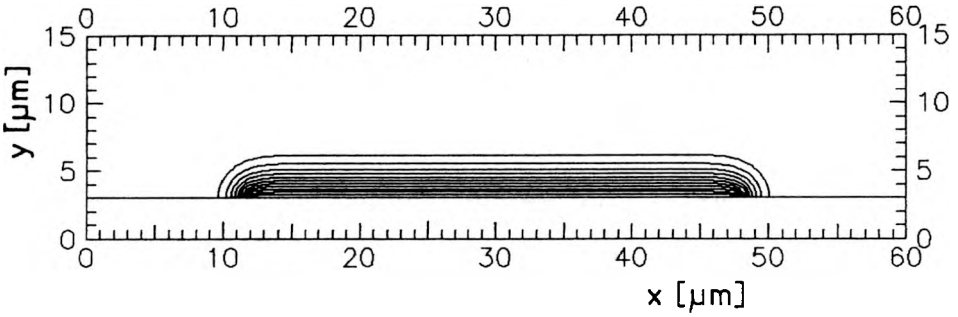


Fig. 2. Distribution of the refractive index profile for the multimode interference structure made by $K^+$-$Na^+$ ion exchange at a time 1 h, for the window width of 36 μm.

multimode in the lateral dimension $x$ (it can support 7 guided modes) for the geometry and technological process parameters chosen in the simulation, and thus only two-dimensional interference effects are observed during the light propagation.

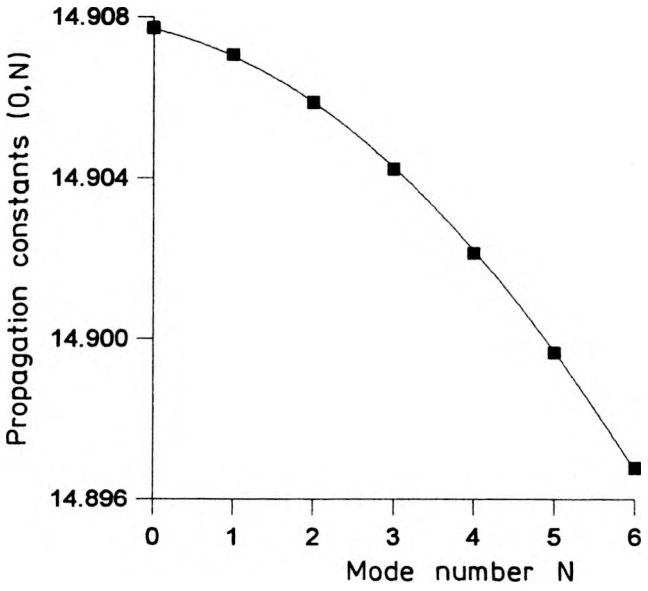


Fig. 3. Propagation constants $\beta(0,N)$ of the multimode ion-exchanged waveguide as a function of mode number $N$. Solid line describes the quadratic function from Eq. (8).

Figure 3 shows dependence of the propagation constants $\beta(0,N)$ on the mode number $N$ determined by the effective index method. The characteristic obtained can be modelled by a quadratic equation

$$\beta(0,N) = 14.9079096 - \pi/(3L_1)N(N+2) \tag{8}$$

where $L_1 = 4572$ μm is the beat length of the two lowest-order modes. Similarly

to the step-index MMI structures nearly quadratic spacing of the propagation constants makes it possible to observe self-imaging phenomena related to general interference as well as restricted paired and restricted symmetric interference [1].

### 4.1. General interference

General interference occurs when all the waveguide modes are excited. Figure 4 presents the wave-field evolution determined by the BPM method from Eq. (7) for MMI structure and excited by the field from a single-mode waveguide. The single-mode waveguide, fabricated for the window opening $w = 8$ μm and time of diffusion $t_D = 1$ h, is situated arbitrarily at 12.9 μm from the structure centre. Figure 5 shows a contour map of the lateral amplitude distribution at $y = 3.3$ μm along the path of propagation $z$, for the propagation length $l_z = 20000$ μm. During

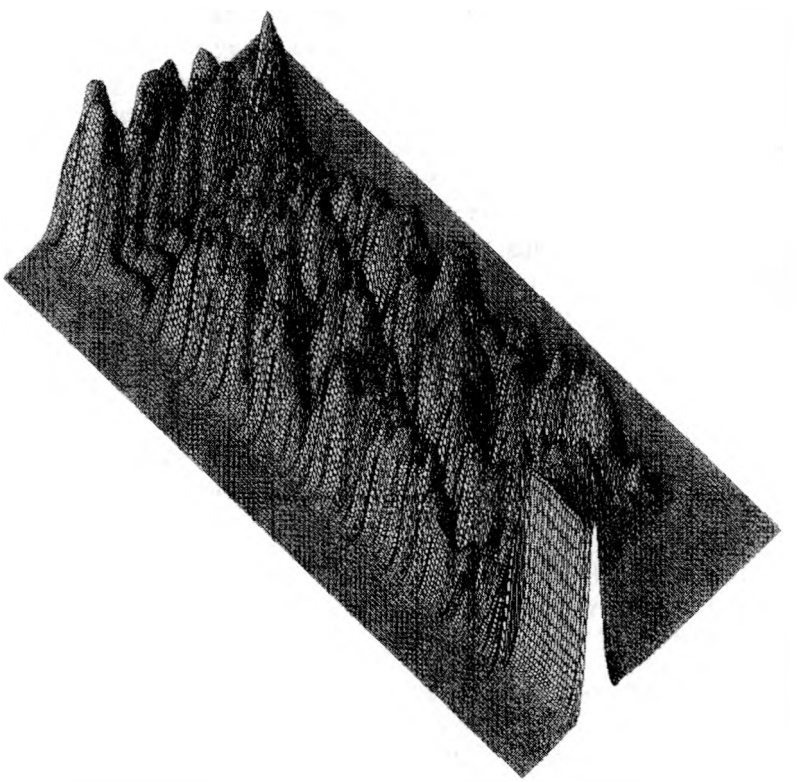

Fig. 4. Field evolution in a gradient multimode section.

the propagation, light passes the distance 2500 μm in the single-mode waveguide and 17500 μm in the MMI section. According to the full modal propagation analysis for the general interference phenomena [1], the input field image mirrored with respect to the MMI symmetry axis is observed at the distance $3L_1$.

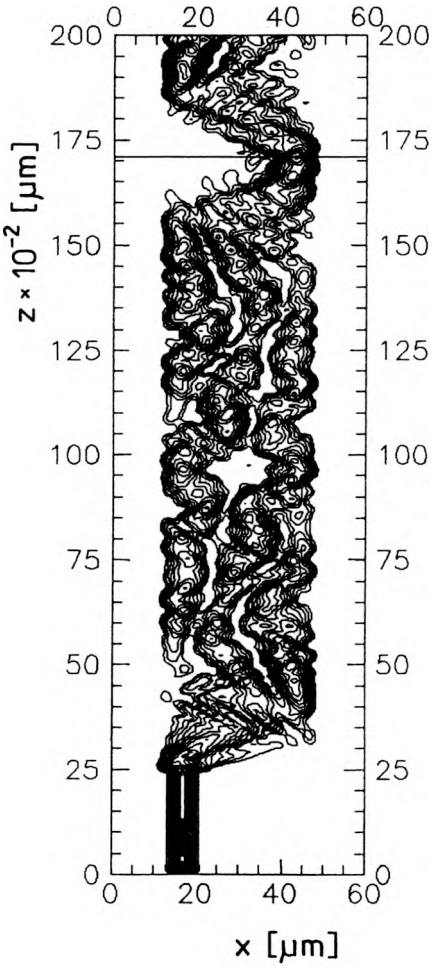


In our simulation, the mirrored image distance marked in Fig. 5 is equal to 14583 μm, which is in good agreement with the $L_1$ value predicted from Eq. (8).

### 4.2. Restricted paired interference

Paired interference occurs when only modes with the mode number $N = 0, 1, 3, 4, 6, 7, \ldots$ are excited. For the step-index structure, a possible way of attaining such a selective excitation is by launching the single-mode input waveguide at 1/3 or 2/3 of the MMI width. In this case, the input field image is at the distance $2L_1$ and its mirror image occurs at $L_1$. At the distance $L_1/n$, multiple images appear, with $n$ being the number of multiple images.

It is assumed for the ion-exchanged MMI structure that the broadening of the refractive index distribution due to the side diffusion can be neglected in relation to the window width. In this case the single-mode waveguide ($w =$ 1.8 μm, $t_D = 1$ h) is placed at 1/3 of the MMI window width. Figure 6 presents a contour map of the lateral amplitude distribution at $y =$ 3.3 μm in the MMI section along the path of propagation determined from Eq. (7) by the BPM method. As the field propagates through the MMI structure, due to the different phase relationships, it starts to split with different

Fig. 5. General interference. Contour map of the lateral field amplitude distribution $A(x, y = 3.3\ \mu m)$ along the path of propagation for the propagation distance $l_z = 20000$ μm. The minimal amplitude contour is equal to 1/6 of the maximum value.

ratios. The characteristic lengths of propagation, where the single, mirror and multiple images appear are marked in the interference pattern. Field distributions at those distances, beginning with the input field at $z = 0$ from the single mode waveguide, are presented in Fig. 7**a**–**d**. One can see from Fig. 7**b** that after the field has propagated a length of $z = 2435$ μm, a distance slightly longer than $L_1/2$, it is divided nearly equally into two parts. The amplitude heights in the left and right arms are equal to $0.614A_0$ and $0.6A_0$, where $A_0$ is the input field amplitude. This indicates that the MMI structure based on $K^+$-$Na^+$ ion exchange in glass can be used as a 3 dB coupler. Choosing a little different length of propagation, as can be seen from Fig. 6, it is possible to use the MMI structure as a power splitter with a different split ratio.

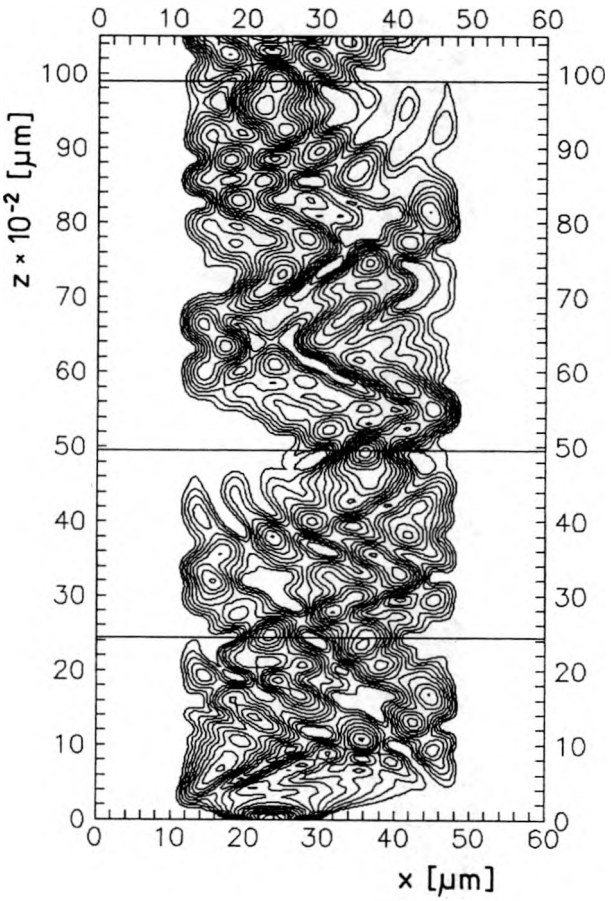


Fig. 6. Restricted paired interference. Contour map of the lateral field amplitude distribution $A(x, y = 3.3\ \mu m)$ along the path of propagation distance $l_z = 10500\ \mu m$. The minimal amplitude contour is equal to 1/6 of the maximum value.

After the field has passed the distance $z = 4935\ \mu m$, which is again a little longer than $L_1$, the mirror image of the input field is observed at 2/3 of the width ofthe MMI structure, as shown in Fig. 7c. The field amplitude is equal to $0.86A_0$. In the next stage of the propagation shown in Fig. 7d, the input field image occurs at the distance $z = 9870\ \mu m$ with the amplitude height of 0.74.

### 4.3. Restricted symmetric interference

Symmetric interference occurs when the MMI section is fed by a single central waveguide. In this case only symmetric modes $N = 0, 2, 4, \ldots$ , are excited. For the step index MMI structures, the input field image appears at the propagation length of $3/4L_1$ and multiple images can be observed at the distance equal to $3/4L_1/n$, where $n$ is the number of multiplications. Figure 8 shows a contour map of the lateral field amplitude distribution at $y = 3.3\ \mu m$ along the propagation distance for the

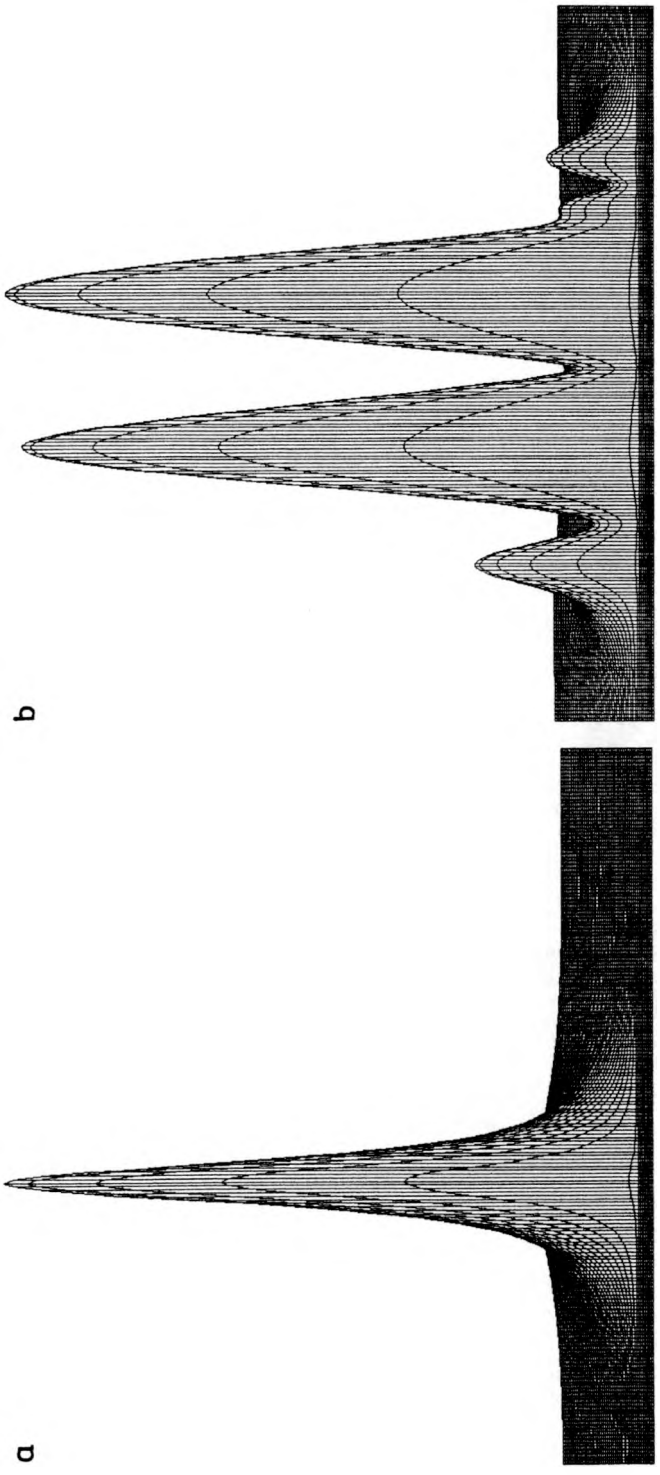
b
a

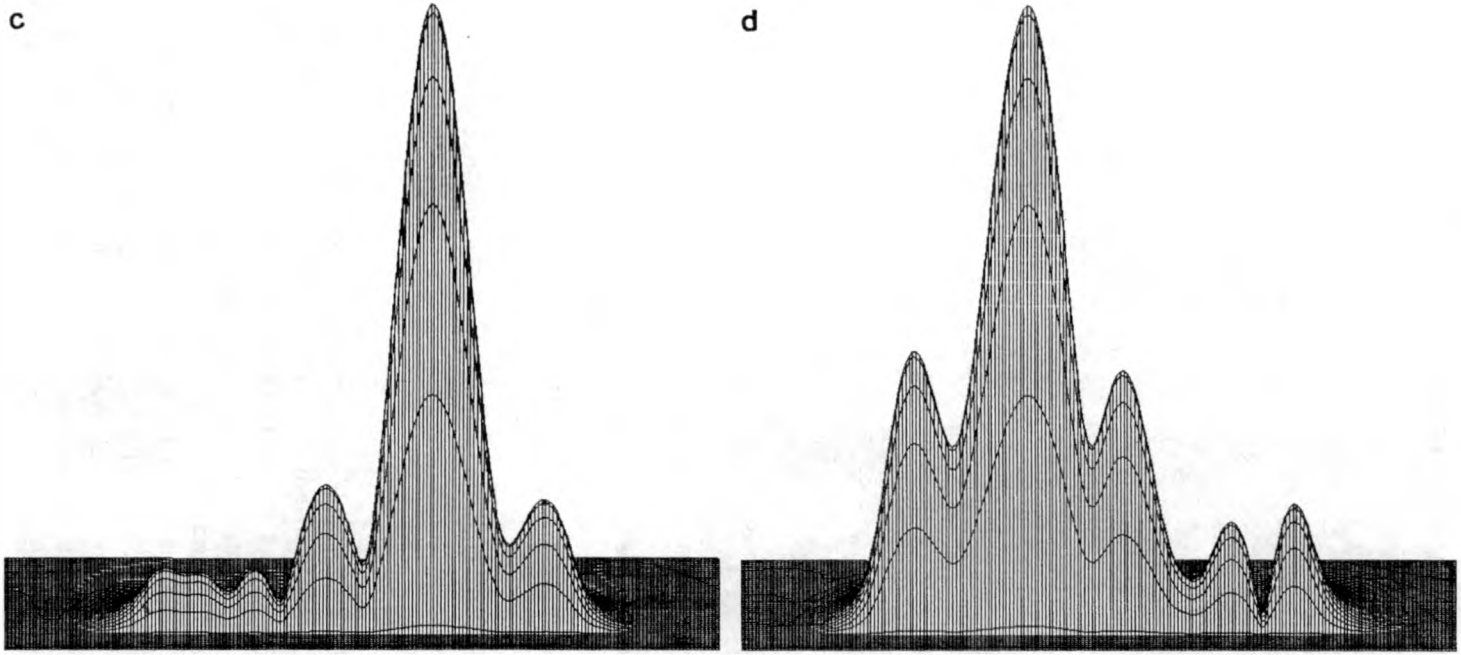


Fig. 7. Input field distribution at $z = 0$ μm (**a**). Restricted paired interference. Field distribution at $z = 2434$ μm (**b**). Restricted paired interference. Field distribution at $z = 4950$ μm (**c**). Restricted paired interference. Field distribution at $z = 9900$ μm (**d**).

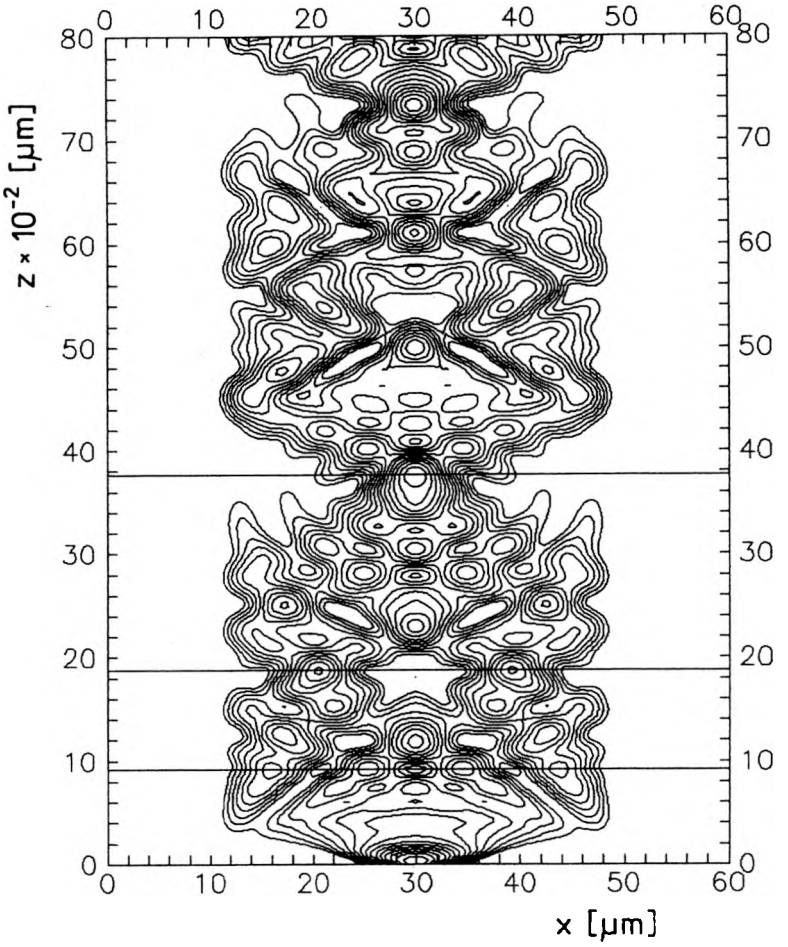


Fig. 8. Restricted symmetric interference. Contour map of the lateral field amplitude distribution $A(x, y = 3.3\ \mu m)$ along the path of propagation for the propagation distance $l_z = 8000\ \mu m$. The minimal amplitude contour is equal to 1/6 of the maximum value.

gradient MMI section excited by the single-mode central waveguide ($w = 1.8\ \mu m$, $t_D = 1$ h). Figures 9**a**–**d** present field distributions for the single and multiple images at propagation lengths marked in Fig. 8. At the distance $z = 920\ \mu m$ (Fig. 9**b**), close to the expected value 3/16 $L_1$, the input field divides into four nearly equal parts of the heights $0.47A_0$, $0.475A_0$, $0.475A_0$ and $0.47A_0$, respectively. This confirms that the ion exchanged MMI structure can be used as a $1 \times 4$ power splitter depending on the MMI section geometry. The $1 \times 2$ power splitting can be realized for the MMI section length of 1880 μm, which is about 3/8 $L_1$, with equal field amplitudes $0.65A_0$ as shown in Fig. 9**c**. Figure 9**d** presents the self-imaging phenomena and the input field reconstruction at the propagation distance $z = 3757\ \mu m$ with the field amplitude of $0.84A_0$.

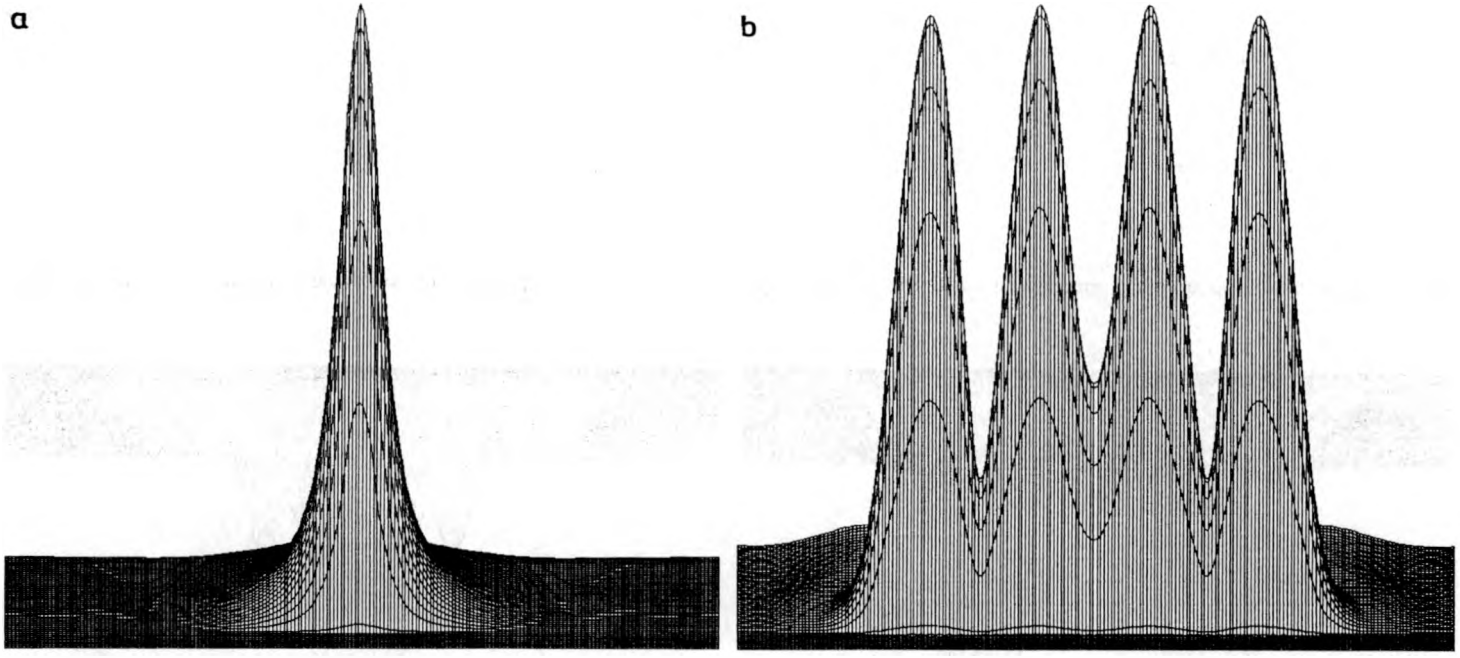


Fig. 9. Input field distribution at $z = 0$ μm (a). Restricted symmetric interference. Field distribution at $z = 920$ μm (b).

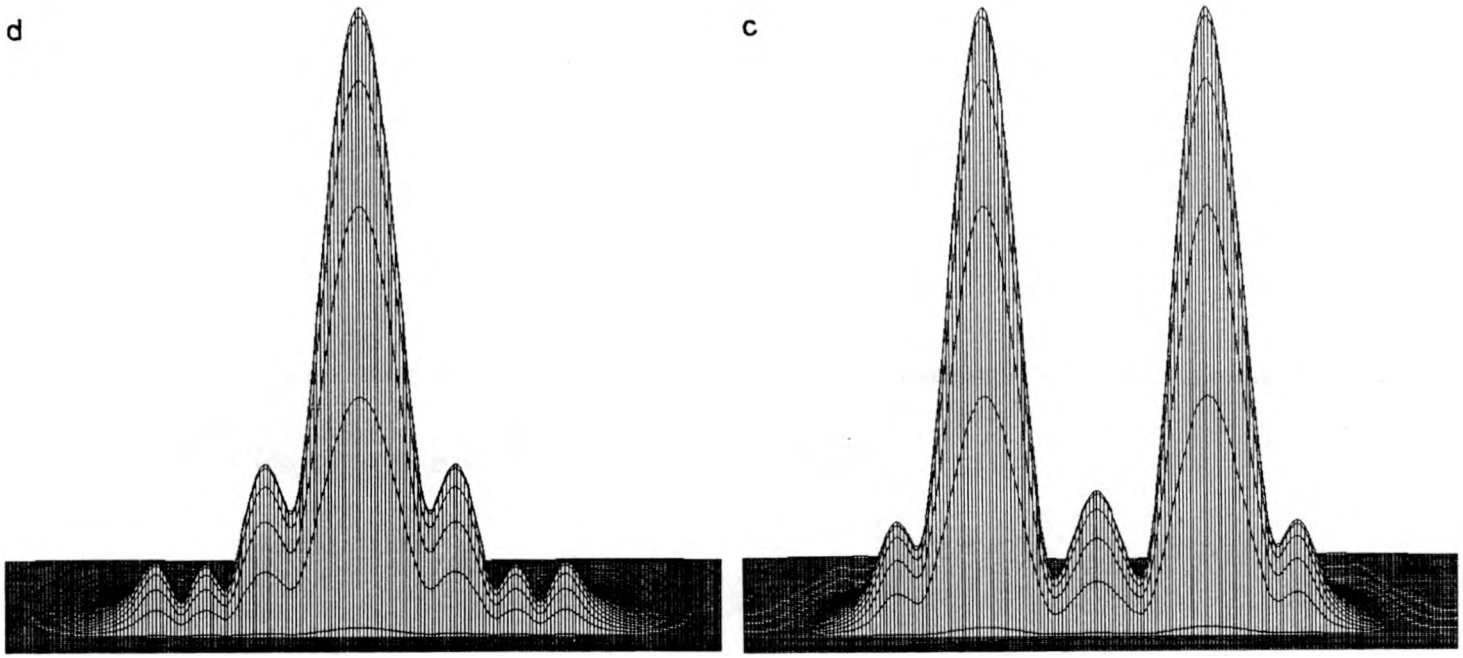


Fig. 9. Restricted symmetric interference. Field distribution at $z = 1880$ μm (c). Restricted symmetric interference. Field distribution $z = 3757$ μm (d).

## 5. Conclusions

The BPM analysis of the gradient MMI structure made by $K^+$-$Na^+$ ion exchange in glass shows a possibility of observing characteristic for the step-index MMI section self-imaging effects connected with the general and restricted interference. During light propagation, single, mirrored, and multiple images of the input field appear at the distances connected with the beat length of the two lowest-order modes. The field distributions presented reproduce the input field image only approximately. The obtained input field images are wider. Also side lobes are visible, as compared to the field at $z = 0$ μm. These effects result from incomplete reconstruction of the input field by the limited number of modal field distributions. Choosing suitable technological process parameters, *i.e.*, window width of the single mode input waveguide and the MMI section geometry, a better adjustment of modal fields can be achieved after optimization. It should also be noted that the imaging quality becomes worse with the increase of the length of wave propagation. This can be explained by a small deviation of the propagation constants from the assumed quadratic dependence on the mode number which tends to blur the reconstructed image field with an increase of the propagation distance. By making MMI structure length as short as possible this effect can be minimized.

Our simulation indicates that the ion-exchange MMI structure examined can be used after certain optimization of the waveguide geometry and technology as a 3 dB coupler and $1 \times N$ power splitter with equal or variable splitting ratio.

### References

[1] SOLDANO L. B., PENNINGS E. C. M., J. Lightwave Technol. **13** (1995), 615.
[2] ULRICH R., ANKELE G., Appl. Phys. Lett. **27** (1975), 337.
[3] RAJARAN M., RAHMAN B. M. A., WONGCHAROEN T., BUAH P. A., GRATTAN K. T. V., Proc. SPIE **2954** (1996), 50.
[4] WIENERT C. M., AGRAWAL N., IEEE Photonic Technol. Lett. **7** (1995), 529.
[5] OPILSKI A., ROGOZIŃSKI R., BŁAHUT M., KARASIŃSKI P., GUT K., OPILSKI Z., Opt. Eng. **36** (1997), 1625.
[6] PRESS W. H., FLANNERY B. P., VETTERLING W. T., *Numerical Recipes: The Art of Scientific Computing*, Cambridge University, New York 1986.
[7] HADLEY G. R., Opt. Lett. **16** (1991), 624.
[8] BŁAHUT M., ROGOZIŃSKI R., GUT K., KARASIŃSKI P., OPILSKI A., Opt. Appl. **24** (1994), 171.

*Received October 28, 1998*